



## Solar photocatalytic abatement of sulfamethoxazole over $\text{Ag}_3\text{PO}_4/\text{WO}_3$ composites



Eleni Grilla<sup>a</sup>, Athanasia Petala<sup>a</sup>, Zacharias Frontistis<sup>a</sup>, Ioannis K. Konstantinou<sup>b</sup>, Dimitris I. Kondarides<sup>a</sup>, Dionissios Mantzavinos<sup>a,\*</sup>

<sup>a</sup> Department of Chemical Engineering, University of Patras, Caratheodory 1, GR-26504 Patras, Greece

<sup>b</sup> Department of Chemistry, University of Ioannina, GR-45110 Ioannina, Greece

### ARTICLE INFO

#### Keywords:

Emerging contaminant  
Hole  
Matrix  
Stability  
Visible

### ABSTRACT

$\text{Ag}_3\text{PO}_4/\text{WO}_3$  composites with  $\text{Ag}_3\text{PO}_4:\text{WO}_3$  molar ratios of 85:15, 75:25, 60:40, 40:60 and 25:75 were synthesized, characterized and tested for the degradation of the antibiotic agent sulfamethoxazole (SMX) under simulated solar radiation. The composites were characterized employing the BET, XRD, UV-vis DRS, SEM-EDS and TEM techniques. Changes in SMX concentration with irradiation time were followed by HPLC.

Of the various materials tested, the  $\text{Ag}_3\text{PO}_4/\text{WO}_3$ (75:25) sample (1  $\text{m}^2/\text{g}$  specific surface area, 2.41 eV band gap energy) exhibited the highest activity with 90% SMX conversion (525  $\mu\text{g}/\text{L}$  initial concentration and 200 mg/L photocatalyst) achieved in just 2 min. Process efficiency was found to increase with increasing photocatalyst concentration (25–200 mg/L) and decreasing SMX concentration (2100–260  $\mu\text{g}/\text{L}$ ). SMX degradation in ultrapure water (UPW) was faster than in bottled water and treated domestic wastewater containing various inorganic and organic constituents; however, certain matrix constituents such as chloride, bicarbonate and humic acid had no or even a positive effect on degradation.

The addition of hydroxyl radical scavengers (t-butanol, DMPO) in excess did not affect SMX degradation, while the opposite phenomenon occurred using a hole scavenger (EDTA), which suppressed degradation. In parallel, no hydroxylated or oxygenated transformation products (TPs) were detected by UPLC-ESI-MS analysis.

The  $\text{Ag}_3\text{PO}_4/\text{WO}_3$ (75:25) sample suffered photo-corrosion resulting in the formation of metallic silver, as well as partial metal leaching in the aqueous phase, both of which contributed to a gradual loss of activity upon repeated use.

### 1. Introduction

Semiconductor photocatalysis has been widely tested to eliminate trace contaminants in water matrices. Since the discovery of  $\text{TiO}_2$  as an effective photo-electrode for water splitting in 1970s, most researchers have focused on  $\text{TiO}_2$  and  $\text{TiO}_2$ -based catalysts for environmental applications, since titania is a photoactive, inexpensive, readily available, stable and non-toxic material. Nonetheless,  $\text{TiO}_2$  photocatalysis suffers a serious drawback associated with its wide bandgap energy (3.0–3.2 eV) which overlaps only with the UV region of the electromagnetic spectrum [1].

In quest of new materials that could be highly responsive in the visible, thus exploiting renewable solar energy to induce photocatalytic reactions, Yi et al. [2] reported for the first time the unique photocatalytic properties of silver orthophosphate ( $\text{Ag}_3\text{PO}_4$ ) for water splitting and the degradation of methylene blue under visible light. This

photocatalyst was substantially more active than other visible light-responsive catalysts, such as  $\text{BiVO}_4$ ,  $\text{WO}_3$  and  $\text{TiO}_{2-x}\text{N}_x$ , since it could achieve a quantum efficiency of up to 90% at wavelengths in the range 400–480 nm, thus implying a very low electron-hole recombination rate [1–3]. Since the pioneering work of Yi et al. [2], some research efforts have focused on the synthesis and characterization of  $\text{Ag}_3\text{PO}_4$ -based materials, whose photocatalytic activity in the visible spectral region has been evaluated using mostly organic dyes as the probe material [4–8].

Our group has recently reported for the first time the use of  $\text{Ag}_3\text{PO}_4$  [9] and  $\text{Ag}_3\text{PO}_4/\text{TiO}_2$  composites [10] for the degradation of trace contaminants of emerging concern, namely xenoestrogens. The rationale behind the use of  $\text{Ag}_3\text{PO}_4/\text{TiO}_2$  composite materials has to do with increased levels of catalyst activity and stability associated with more efficient charge separation, as well as greater specific surface areas of the composites compared to  $\text{Ag}_3\text{PO}_4$ . Complete degradation of 220  $\mu\text{g}/\text{L}$

\* Corresponding author.

E-mail address: [mantzavinos@chemeng.upatras.gr](mailto:mantzavinos@chemeng.upatras.gr) (D. Mantzavinos).

bisphenol A using a composite with a  $\text{Ag}_3\text{PO}_4:\text{TiO}_2$  molar ratio of 75:25 could be achieved in just 4 min of simulated solar irradiation, i.e. over three times faster than with Evonik P-25  $\text{TiO}_2$  and twice faster than with pure  $\text{Ag}_3\text{PO}_4$  [10].

A major issue associated with  $\text{Ag}_3\text{PO}_4$  is its photochemical instability since, in the absence of appropriate electron scavengers in the solution, the photocatalyst is irreversibly reduced to metallic silver [2,11]. This was observed in our previous work [10], where silver ion reduction occurred for both pure  $\text{Ag}_3\text{PO}_4$  and  $\text{Ag}_3\text{PO}_4/\text{TiO}_2$  catalysts; however, the latter retained greater catalytic activity than the former. Zhang et al. [12] synthesized  $\text{Ag}_3\text{PO}_4/\text{WO}_3$  composites and tested them for the decomposition of organic dyes under visible light radiation. They found that the composites were substantially more active than their individual components for the above reaction and, more importantly, they suffered minimum silver ion reduction to metallic silver (although reduction was not completely impeded). Since the conduction band (CB) minimum of tungsten trioxide (0.64 V vs. NHE) is more positive in the electrochemical scale than that of  $\text{Ag}_3\text{PO}_4$  (0.45 V vs. NHE), the photogenerated electrons are expected to move from the CB of  $\text{Ag}_3\text{PO}_4$  to that of  $\text{WO}_3$ , which would avoid the formation of metallic silver on the surface of the photocatalyst [11]. Similarly, Chang et al. [13] reported only 5% metallic silver formation on the surface of a  $\text{Ag}_3\text{PO}_4/\text{WO}_3$  composite used for rhodamine photocatalytic degradation, while the respective value was over 27% for pure  $\text{Ag}_3\text{PO}_4$ .

In this perspective, our group synthesized, characterized and tested  $\text{Ag}_3\text{PO}_4/\text{WO}_3$  composite materials of variable  $\text{Ag}_3\text{PO}_4:\text{WO}_3$  content for the photocatalytic degradation of sulfamethoxazole (SMX), a pharmaceutical agent belonging to the group of sulfonamide antibiotics. SMX was chosen as a model trace contaminant since it is probably the most commonly employed antibiotic of this group and it is widely prescribed to treat human and animal infections. The fate of antibiotics, amongst other pharmaceuticals, in the aquatic environment (their occurrence has been reported in surface water, seawater, groundwater, as well as in soils and sediments [14,15]) has attracted enormous attention in recent years because antibiotics are biologically active and, therefore, they cannot be efficiently removed in conventional wastewater treatment plants. Moreover, the increase in antibiotics consumption and their subsequent release into the environment over the past few decades has resulted in the generation of bacteria that are strongly resistant to antibiotics [16,17].

Although there have been a few studies regarding the use of  $\text{Ag}_3\text{PO}_4/\text{WO}_3$  composite materials for the photocatalytic degradation of organic dyes and phenol [12,13,18–20], this is, to the best of our knowledge, the first report on the degradation of a pharmaceutical micro-contaminant of environmental concern by photocatalysis over  $\text{Ag}_3\text{PO}_4/\text{WO}_3$  composites or, indeed, any other  $\text{Ag}_3\text{PO}_4$ -based material.

In this work, the influence of catalyst composition and of process parameters, such as catalyst concentration, antibiotic concentration, type of radiation and quality of actual and synthetic water matrices on SMX degradation kinetics was investigated. Issues associated with degradation pathways and catalyst stability are also discussed.

## 2. Materials and methods

### 2.1. Chemicals and water matrices

Sulfamethoxazole (SMX:  $\text{C}_{10}\text{H}_{11}\text{N}_3\text{O}_3\text{S}$ ) was purchased from Sigma-Aldrich (CAS no: 72 3-4 6-6) and used as received. Sodium tungstate dihydrate ( $\text{Na}_2\text{WO}_4\cdot\text{H}_2\text{O}$ , CAS no: 10213-10-2) and ammonium chloride ( $\text{NH}_4\text{Cl}$ , CAS no: 12125-02-9) were supplied by Sigma-Aldrich, silver nitrate ( $\text{AgNO}_3$ , CAS no: 7761-88-8) was supplied by Alfa Aesar and sodium dihydrogen phosphate monohydrate ( $\text{NaH}_2\text{PO}_4\cdot\text{H}_2\text{O}$ , CAS no: 10049-21-5) was supplied by Merck Millipore. Ethylenediaminetetraacetic acid (EDTA, CAS no: 60-00-4) and t-butanol (CAS no: 75-65-0) were purchased from Sigma-Aldrich, while 5,5-dimethyl-1-pyrroline-N-oxide (DMPO, CAS no: 3317-61-1) was

purchased from Cayman Chemical.

Most of the experiments reported here were carried out in ultrapure water (UPW, pH = 6) taken from a water purification system (EASYPure RF-Barnstead/Thermolyne, USA). Other matrices included (i) commercially available bottled water (BW: pH = 7.6, 475  $\mu\text{S}/\text{cm}$  conductivity containing 286 mg/L bicarbonate, 8.2 mg/L chloride, 9.6 mg/L sulfate, 7.9 mg/L nitrate and 102.7 mg/L various metal ions), (ii) secondary treated wastewater (WW) taken from the university campus treatment plant (pH = 8, total organic carbon = 8.8 mg/L), and (iii) UPW spiked with various water constituents such as humic acid (CAS number 1415-93-6), bicarbonate (CAS no: 144-55-8) and chloride (CAS no: 7647-14-5); all of them were purchased from Sigma-Aldrich.

### 2.2. Preparation of photocatalysts

The  $\text{Ag}_3\text{PO}_4/\text{WO}_3$  composites were prepared by a deposition-precipitation process. An appropriate amount of  $\text{Na}_2\text{WO}_4\cdot\text{H}_2\text{O}$  was dissolved in 25 mL of triply distilled water (solution A), whereas 1.91 g of  $\text{NaH}_2\text{PO}_4$  was dissolved in 25 mL of UPW (solution B). After stirring for 15 min, solutions A and B were added in an aqueous solution (50 mL) of  $\text{AgNO}_3$  (3.06 g). The resulting mixture was left under vigorous stirring for 4 h at room temperature. The obtained precipitate was collected by filtration, washed with triply distilled water for several times and then dried in an oven at 60 °C for 12 h. Composites with different molar ratios of  $\text{Ag}_3\text{PO}_4$  to  $\text{WO}_3$  were prepared varying the amount of  $\text{Na}_2\text{WO}_4\cdot\text{H}_2\text{O}$  in the starting solution, while keeping constant the content of  $\text{Ag}_3\text{PO}_4$ . The photocatalysts thus prepared are denoted in the following as  $\text{Ag}_3\text{PO}_4/\text{WO}_3$  (x:y), where x:y is the molar ratio of  $\text{Ag}_3\text{PO}_4$  to  $\text{WO}_3$ .

Pure  $\text{Ag}_3\text{PO}_4$  was prepared using the same method but in the absence of  $\text{Na}_2\text{WO}_4\cdot\text{H}_2\text{O}$ .

Pure  $\text{WO}_3$  was prepared according to a hydrothermal method reported by Zhang et al [12]. Briefly, appropriate amounts of  $\text{Na}_2\text{WO}_4\cdot\text{H}_2\text{O}$  (0.05 M) and  $\text{NH}_4\text{Cl}$  (0.5 M) aqueous solutions were mixed and placed in a 90 mL teflon-lined stainless steel autoclave and kept at 180 °C for 48 h. The precipitate was obtained by centrifugation, washed with distilled water and dried at 70 °C for 12 h. Finally,  $\text{WO}_3$  was obtained after calcination at 500 °C for 2 h.

### 2.3. Catalyst characterization

The as prepared photocatalysts were characterized by (i) X-Ray diffraction (XRD) using a Philips P (PW 1830/40) instrument employing Cu Ka source ( $\lambda = 1.5406 \text{ \AA}$ ), (ii) nitrogen physisorption at liquid nitrogen temperature (B.E.T. method) on a Micromeritics Gemini III 2375 analyzer, (iii) UV-vis diffuse reflectance spectroscopy (DRS) in the range of 200–800 nm with a UV-vis spectrophotometer (Varian Cary 3), (iv) scanning electron microscopy (SEM) using a JEOL 6300 microscope equipped with an energy dispersive spectrometer (EDS), and (v) transmission electron microscopy (TEM) with a JEOL JEM-2100 system, operated at 200 kV. The characterization techniques and procedures have been described in detail elsewhere [10].

### 2.4. Experimental procedure

In a typical run, 120 mL of an aqueous solution containing, unless otherwise stated, 525  $\mu\text{g}/\text{L}$  SMX were loaded in the cylindrical reaction vessel under continuous stirring at 400 rpm. This SMX concentration was chosen to (i) match realistically those typically found in environmental samples (i.e. between ng/L and low  $\mu\text{g}/\text{L}$  levels), and (ii) facilitate SMX quantitation with the analytical protocols/techniques available in this work. The appropriate amount of catalyst was then added and the solution was left to equilibrate in the dark for 15 min. The solar simulator (Oriel, model LCS 100 equipped with a 100 W xenon, ozone-free lamp) was then turned on and samples of 1.2 mL were periodically

taken from the reactor, filtered with a  $0.2\text{ }\mu\text{m}$  PVDF Whatman syringe filter and analyzed by liquid chromatography.

Simulated solar radiation contains about 5% UVA radiation, and 0.1% UVB radiation. In addition, an optic filter (Newport FSQ-UG5,  $50.8\text{ mm} \times 50.8\text{ mm}$ ) was used to provide the visible part of solar spectrum, cutting photons with wavelengths below  $420\text{ nm}$ . The incident radiation intensity on the photochemical reactor in the UV region of the electromagnetic spectrum was measured using ferrioxalate as the chemical actinometer and it was found to be  $1.3 \times 10^{-4}$  einstein/( $\text{m}^2\text{ s}$ ). For the runs performed under visible light, the intensity was measured at  $7 \times 10^{-5}$  einstein/( $\text{m}^2\text{ s}$ ).

### 2.5. Analytical techniques

High performance liquid chromatography (HPLC:Waters Alliance 2695) was used to analyze SMX concentration. Separation was achieved on a Kinetex XB-C18 100A column ( $2.6\text{ }\mu\text{m}$ ,  $2.1\text{ mm} \times 50\text{ mm}$ ) and a  $0.5\text{ }\mu\text{m}$  inline filter (KrudKatcher Ultra). The mobile phase consisting of 68:32 UPW:acetonitrile eluted isocratically at  $0.32\text{ mL/min}$  and  $45^\circ\text{C}$ . The injection volume was  $20\text{ }\mu\text{L}$ , while the detection was through a UV-vis detector (Waters 2996) set at  $270\text{ nm}$ .

To identify transformation products (TPs), samples ( $5\text{ mL}$ ) were pre-concentrated by solid phase extraction using Oasis cartridges ( $3\text{ mL}$ ,  $60\text{ mg}$ ). The extracts were analyzed by an ultra performance liquid chromatography - electrospray ionization - mass spectrometry (UPLC-ESI-MS) system, which includes Accela autosampler, Accela LC pump and LTQ Orbitrap mass spectrometer (Thermo Fisher Scientific, Germany) and is operated in positive ionization mode. The chromatographic separation was conducted using a C18 Speed Core PFP column, ( $50\text{ mm} \times 2.1\text{ mm}$ ,  $2.6\text{ }\mu\text{m}$  particle size (Fortis Technologies Ltd)), thermo-stated at  $30^\circ\text{C}$ . Injection volume was  $10\text{ }\mu\text{L}$  and flow rate  $300\text{ }\mu\text{L/min}$ . More details about the procedures are given as supplementary information.

Inductively coupled plasma mass spectrometry (ICP-MS) (Agilent Technologies, 7500 series) was employed to determine the concentration of leached silver in the aqueous phase.

## 3. Results and discussion

### 3.1. Catalyst characterization

Fig. 1 shows the XRD patterns of the as-synthesized  $\text{Ag}_3\text{PO}_4/\text{WO}_3$  composites and the single-component  $\text{Ag}_3\text{PO}_4$  and  $\text{WO}_3$  samples. It is observed that all the diffraction peaks of pure  $\text{Ag}_3\text{PO}_4$  (trace a) can be attributed to the body-centered cubic phase of  $\text{Ag}_3\text{PO}_4$  (JCPDS 01-1058), whereas in the case of  $\text{WO}_3$  (trace g) all diffraction peaks correspond to the monoclinic phase of  $\text{WO}_3$  (JCPDS No. No.43-1035). The XRD pattern of  $\text{Ag}_3\text{PO}_4/\text{WO}_3(85:15)$ , i.e. the composite sample with the lowest  $\text{WO}_3$  loading, contains only peaks due to  $\text{Ag}_3\text{PO}_4$  (trace b). The absence of reflections attributable to  $\text{WO}_3$  indicates that this component is either very well dispersed and/or not well crystallized. Increase of  $\text{WO}_3$  molar content to 25% results in the appearance of XRD peaks due to both  $\text{Ag}_3\text{PO}_4$  and  $\text{WO}_3$  phases (trace c). The fact that the positions of these peaks are the same with those of the single-component samples (traces a and g, respectively) indicates that  $\text{WO}_3$  is not incorporated into the  $\text{Ag}_3\text{PO}_4$  lattice [20] and that there is no strong chemical interaction between the two phases. Further increase of the  $\text{WO}_3$  molar content to 40% or 60% (trace d) or 60% (trace e) results in the disappearance of reflections attributable to  $\text{WO}_3$  and in a decrease of the intensity of XRD peaks corresponding to  $\text{Ag}_3\text{PO}_4$ , indicating the poor crystallinity of the materials. Interestingly, the  $\text{Ag}_3\text{PO}_4/\text{WO}_3(25:75)$  sample with the highest  $\text{WO}_3$  content is, practically, amorphous as indicated by the absence of clear reflections in the XRD pattern (trace f).

The mean primary crystallite size,  $d$ , of the phases detected in the XRD patterns of Fig. 1 was estimated according to Scherrer equation [10]. Results showed that the crystallite size of the single-component

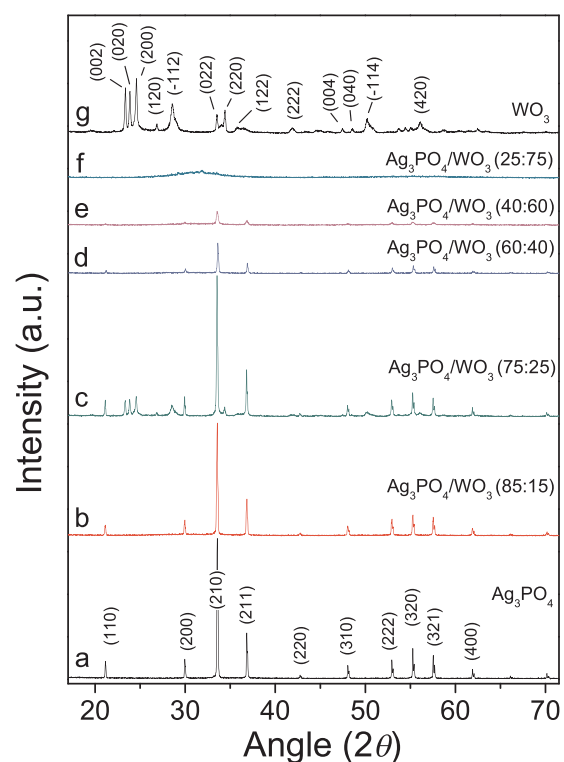


**Fig. 1.** X-ray diffraction patterns of  $\text{Ag}_3\text{PO}_4$ ,  $\text{WO}_3$  and  $\text{Ag}_3\text{PO}_4/\text{WO}_3$  composites with variable composition. Reflections indexed to the body-centered cubic phase of  $\text{Ag}_3\text{PO}_4$  and to the monoclinic phase of  $\text{WO}_3$  are shown in parentheses.

$\text{Ag}_3\text{PO}_4$  and  $\text{WO}_3$  samples was  $58\text{ nm}$  and  $48\text{ nm}$ , respectively. Similar values were obtained for all composite catalysts investigated, with the exception of the  $\text{Ag}_3\text{PO}_4/\text{WO}_3(40:60)$  sample (supplementary information, Table S1). The specific surface area was relatively low for all samples and varied in the range  $1\text{--}5\text{ m}^2/\text{g}$  (Table S1).

The morphology and elemental composition of the as synthesized photocatalysts were examined by SEM/EDS and representative results obtained for  $\text{Ag}_3\text{PO}_4$ ,  $\text{WO}_3$ ,  $\text{Ag}_3\text{PO}_4/\text{WO}_3(75:25)$  samples are shown in Fig. 2(A–C). It is observed that the  $\text{Ag}_3\text{PO}_4$  photocatalyst (Fig. 2A) consists of spherical particles with an average size of  $\sim 2\text{ }\mu\text{m}$ . The  $\text{WO}_3$  photocatalyst is also composed of spherical-like particles ( $\sim 2\text{--}3\text{ }\mu\text{m}$ ), which tend to agglomerate (Fig. 2B). A similar morphology is observed for the  $\text{Ag}_3\text{PO}_4/\text{WO}_3(75:25)$  sample (Fig. 2C), whose EDS pattern (Fig. 2D) indicates the presence of the elements O, P, Ag and W, which are evenly distributed on the photocatalyst surface (Fig. 2E and F). Qualitatively similar results were obtained for all  $\text{Ag}_3\text{PO}_4/\text{WO}_3(x:y)$  samples investigated (supplementary information, Fig. S1).

Fig. 3A shows a representative high resolution TEM image of  $\text{Ag}_3\text{PO}_4/\text{WO}_3(75:25)$ . Clear lattice fringes are detected, indicating the relatively good crystallinity of the as prepared photocatalyst. More specifically, two different lattice fringes are clearly discerned (Fig. 3B) with a spacing of about  $0.26\text{ nm}$  and  $0.38\text{ nm}$ , corresponding to the  $(210)$  lattice spacing of  $\text{Ag}_3\text{PO}_4$  and the  $(002)$  lattice spacing of  $\text{WO}_3$ , respectively [21]. This observation demonstrates the intimate contact between the two phases in the composite photocatalyst, which is expected to facilitate the charge transfer between the two semiconductors.

The DRS spectra of the studied photocatalysts are shown in Fig. 4. It is observed that  $\text{Ag}_3\text{PO}_4$  absorbs light at wavelengths below  $\sim 530\text{ nm}$  (trace a) and that absorption in the visible decreases progressively with increase of  $\text{WO}_3$  content (traces b–f). The  $\text{WO}_3$  sample (trace g) has an absorption threshold at  $\sim 470\text{ nm}$ , which is in agreement with previously reported data for the  $\text{WO}_3$  orthorhombic structure [12]. The optical band gaps of the synthesized materials were estimated

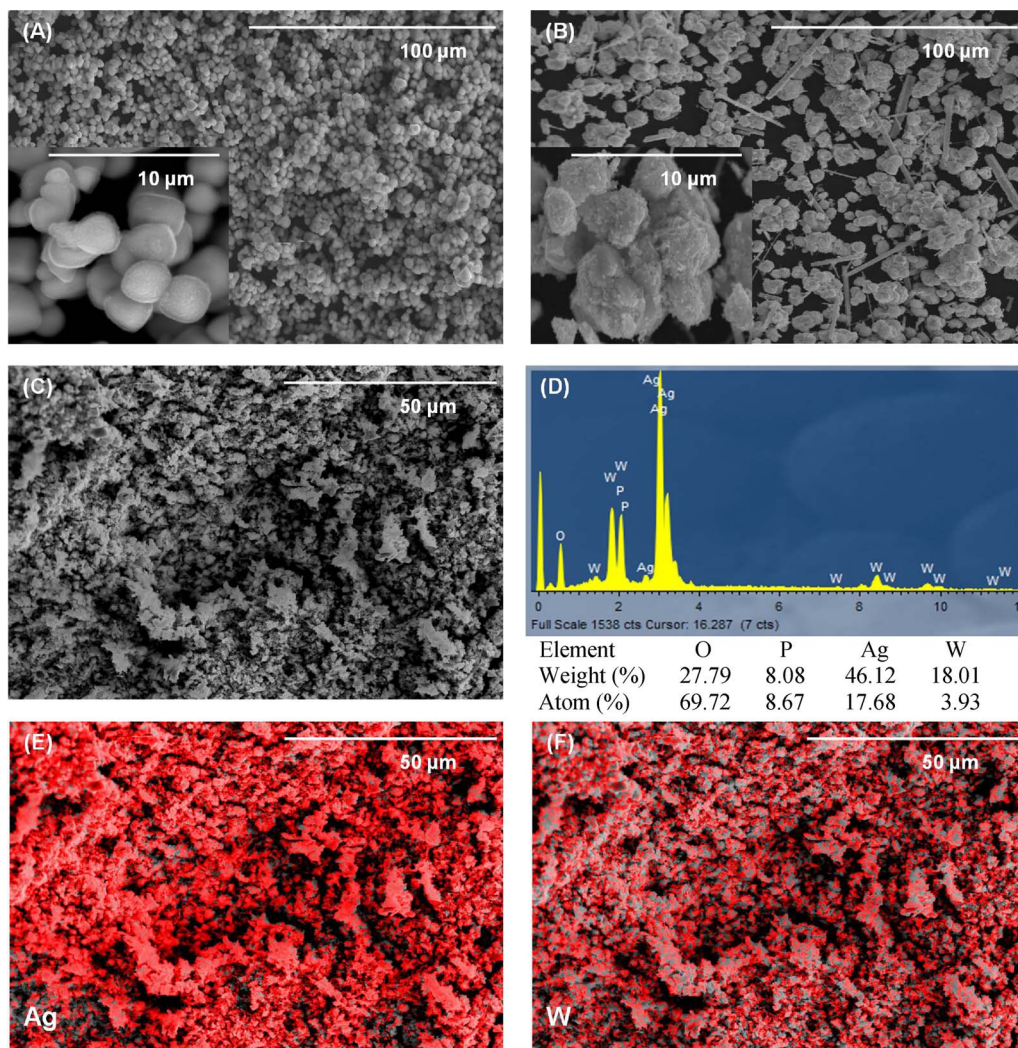


**Fig. 2.** SEM images of (A)  $\text{Ag}_3\text{PO}_4$ , (B)  $\text{WO}_3$  and (C)  $\text{Ag}_3\text{PO}_4/\text{WO}_3(75:25)$  photocatalysts. (D) EDS spectrum obtained from  $\text{Ag}_3\text{PO}_4/\text{WO}_3(75:25)$  sample and EDS mapping results showing the distribution of (E) Ag and (F) W elements.

according to the Tauc method [22] and typical results obtained are shown in Fig. 5. It is observed that the band gap of  $\text{Ag}_3\text{PO}_4$  (trace a) and  $\text{WO}_3$  (trace c) is 2.41 eV and 2.65 eV, respectively, in agreement with literature results [12,20]. Regarding the  $\text{Ag}_3\text{PO}_4/\text{WO}_3(75:25)$  sample (trace b), the band gap was 2.41 eV, i.e. similar to that of pristine  $\text{Ag}_3\text{PO}_4$ . Qualitatively similar results were obtained for all  $\text{Ag}_3\text{PO}_4/\text{Ag}_3\text{PO}_4$

$\text{WO}_3$  composites investigated (Table S1).

### 3.2. Evaluation of catalyst activity

To assess whether the composite materials and their individual components exhibit photocatalytic activity towards SMX degradation

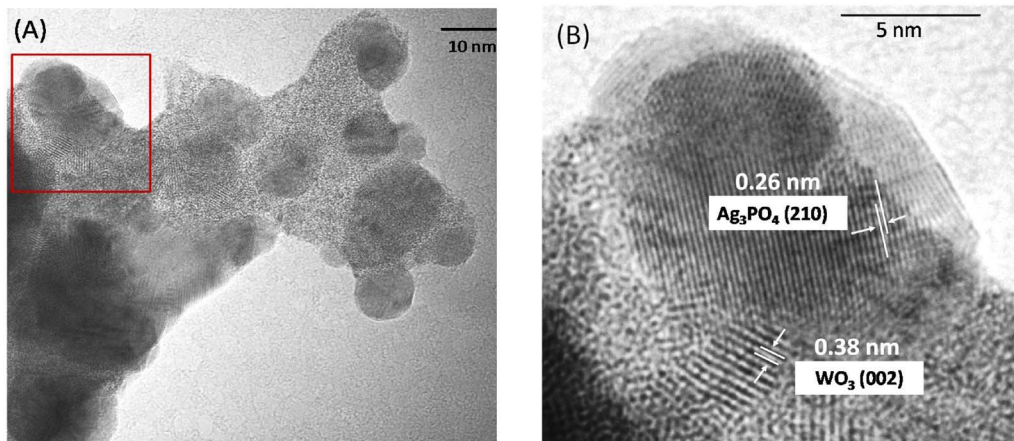


**Fig. 3.** (A) HRTEM image and (B) a magnified view of  $\text{Ag}_3\text{PO}_4/\text{WO}_3(75:25)$  photocatalyst.

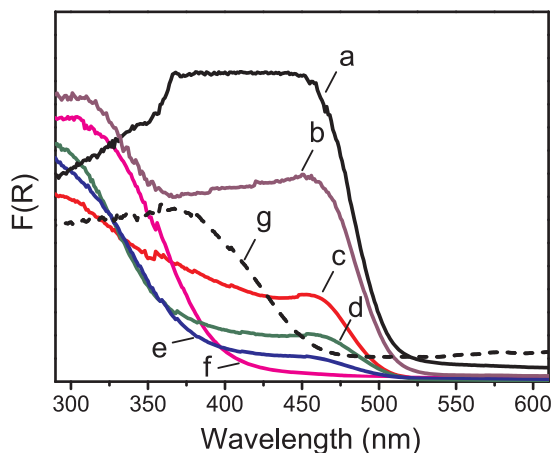


**Fig. 4.** UV-vis diffuse reflectance spectra obtained for: (a)  $\text{Ag}_3\text{PO}_4$ , (b)  $\text{Ag}_3\text{PO}_4/\text{WO}_3$ (85:15), (c)  $\text{Ag}_3\text{PO}_4/\text{WO}_3$ (75:25), (d)  $\text{Ag}_3\text{PO}_4/\text{WO}_3$ (60:40), (e)  $\text{Ag}_3\text{PO}_4/\text{WO}_3$ (40:60); (f)  $\text{Ag}_3\text{PO}_4/\text{WO}_3$ (25:75) and (g)  $\text{WO}_3$ .

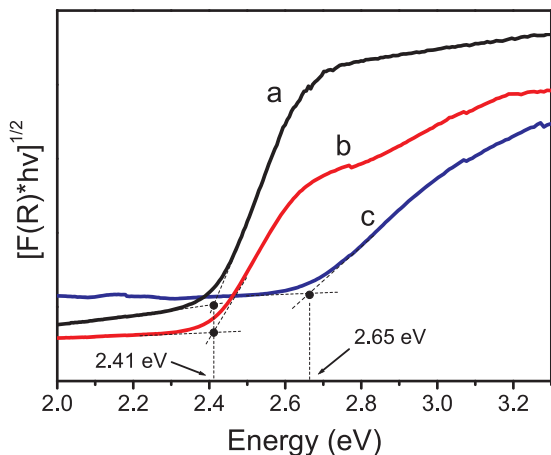


**Fig. 5.** Tauc plots obtained from the UV-vis diffuse reflectance spectra of Fig. 4 for (a)  $\text{Ag}_3\text{PO}_4$ , (b)  $\text{Ag}_3\text{PO}_4/\text{WO}_3$ (75:25) and (c)  $\text{WO}_3$ .

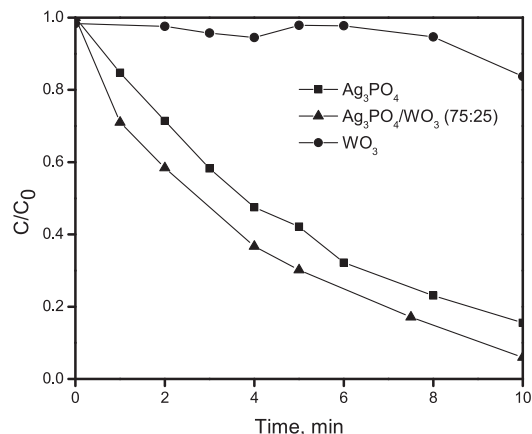


**Fig. 6.** Photocatalytic activity of 100 mg/L  $\text{Ag}_3\text{PO}_4$ ,  $\text{WO}_3$  and their composite for the degradation of 525  $\mu\text{g}/\text{L}$  SMX in UPW.

under simulated solar radiation, preliminary experiments were conducted with  $\text{Ag}_3\text{PO}_4$ ,  $\text{WO}_3$  and  $\text{Ag}_3\text{PO}_4/\text{WO}_3$  (75:25) at 100 mg/L catalyst concentration and the results are shown in Fig. 6. Both pure  $\text{Ag}_3\text{PO}_4$  and its composite are capable of degrading SMX, while pure  $\text{WO}_3$  has practically no activity at the conditions in question. To quantify reaction rates, SMX degradation is assumed to follow a pseudo-first order kinetic expression:

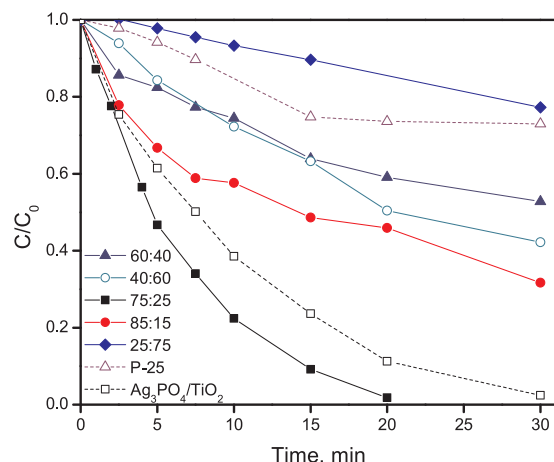


**Fig. 7.** Photocatalytic activity of 50 mg/L  $\text{Ag}_3\text{PO}_4/\text{WO}_3$  samples with the indicated  $\text{Ag}_3\text{PO}_4/\text{WO}_3$  molar ratios for the degradation of 525  $\mu\text{g}/\text{L}$  SMX in UPW. Background runs with  $\text{P}-25 \text{ TiO}_2$  and  $\text{Ag}_3\text{PO}_4/\text{TiO}_2$ (75:25) are also included (dashed lines).

$$-\frac{dC}{dt} = kC \Rightarrow \ln\left(\frac{C_0}{C}\right) = k_{app}t \quad (1)$$

where  $C$  and  $C_0$  is SMX concentration at time  $t = t$  and  $t = 0$ , respectively and  $k_{app}$  is an apparent rate constant incorporating the relatively constant concentration of oxidizing species. Applying Eq. (1) for SMX conversion up to 90%, the computed  $k_{app}$  values are 0.184 (0.998) and 0.244  $\text{min}^{-1}$  (0.993) for pure  $\text{Ag}_3\text{PO}_4$  and its composite, respectively; the numbers in parentheses show the values of linear regression coefficients.

In our previous work concerning the solar photocatalytic degradation of bisphenol A over various  $\text{Ag}_3\text{PO}_4/\text{TiO}_2$  composites [10], it was found that the reactivity was dependent on the molar ratio of  $\text{Ag}_3\text{PO}_4$  to  $\text{TiO}_2$ . Similarly, the rate of SMX degradation appears to be a function of  $\text{Ag}_3\text{PO}_4$  to  $\text{WO}_3$  molar ratio, as depicted in Fig. 7; the computed  $k_{app}$  values are 0.154, 0.042, 0.031, 0.025 and 0.008  $\text{min}^{-1}$  for the composites with 75:25, 85:15, 40:60, 60:40 and 25:75 molar ratios. The substantially better performance of the 75:25 composite may be ascribed to its greater crystallinity compared to all other samples.

An additional experiment was performed with Evonik P-25  $\text{TiO}_2$ , a benchmark photocatalyst in most environmental applications; its activity ( $0.016 \text{ min}^{-1}$ ) is substantially lower than that of  $\text{Ag}_3\text{PO}_4$  although its SSA of  $50 \text{ m}^2/\text{g}$  is about 25 times greater. Fig. 7 also shows an experiment with a  $\text{Ag}_3\text{PO}_4/\text{TiO}_2$ (75:25) material prepared and tested in our previous work [10]; its activity ( $0.102 \text{ min}^{-1}$ ) is about a third lower than that of  $\text{Ag}_3\text{PO}_4/\text{WO}_3$  (75:25).

In view of these screening trials, all subsequent experiments were performed with the  $\text{Ag}_3\text{PO}_4/\text{WO}_3$ (75:25) composite catalyst.

### 3.3. Effect of catalyst concentration and radiation type

The effect of increasing catalyst concentration in the range 25–200 mg/L on SMX degradation under solar and visible radiation is shown in Fig. 8A and B, respectively, while Fig. 8C summarizes the corresponding apparent rate constants. Degradation increases with increasing catalyst concentration, which is characteristic of a heterogeneous photocatalytic regime where the rate depends on the photocatalyst sites available for reaction [23]. To confirm that SMX degradation is owing to interactions between photons and the catalyst surface, an additional experiment was performed without catalyst yielding only 22% removal after 20 min of solar irradiation (Fig. 8A).

Although the reaction occurs to a considerable extent under visible light only (Fig. 8B), the contribution of the ultraviolet part of the solar spectrum appears to be important and this is more pronounced at the lower catalyst concentrations. For example, the rate of degradation

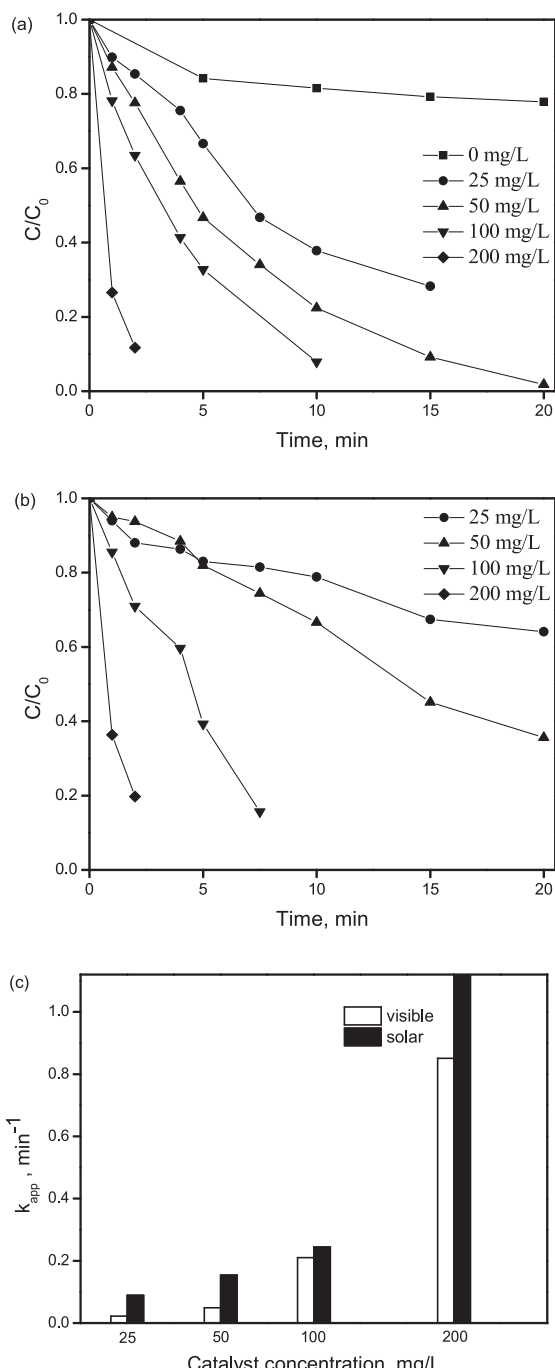


**Fig. 8.** Effect of  $\text{Ag}_3\text{PO}_4/\text{WO}_3(75:25)$  concentration on 525  $\mu\text{g/L}$  SMX degradation in UPW under (a) solar radiation and (b) visible radiation. (c) Relationship between apparent rate constant and catalyst concentration.

under solar radiation is 3–4 times greater than in the visible at 25–50 mg/L catalyst, but the two rates become comparable at 100–200 mg/L catalyst.

#### 3.4. Effect of SMX concentration

The effect of changing SMX concentration in the range 260–2100  $\mu\text{g/L}$  on its degradation is shown in Fig. 9. The computed apparent rate constants are 0.278, 0.154, 0.026 and 0.012  $\text{min}^{-1}$  at 260, 525, 1050 and 2100  $\mu\text{g/L}$  concentration, which implies that the reaction is not true first order with respect to SMX concentration although data fitting to Eq. (1) is still good. As a matter of fact, SMX

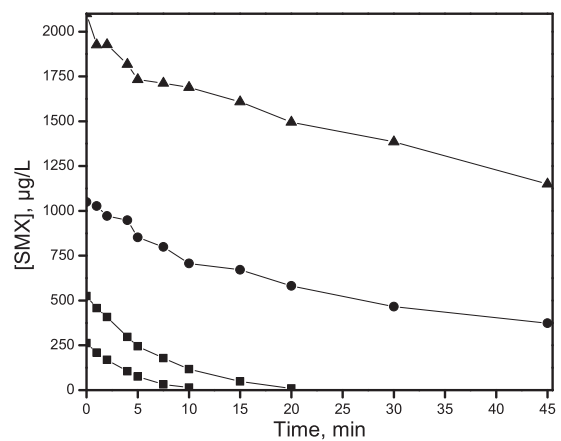


**Fig. 9.** Effect of SMX concentration on its degradation with 50 mg/L  $\text{Ag}_3\text{PO}_4/\text{WO}_3(75:25)$  in UPW.

conversion decreases with increasing concentration, e.g. its 5-min value is 72%, 53% and 19% at 260, 525 and 1050  $\mu\text{g/L}$  concentration, respectively and the 30-min value is 56% and 34% at 1050 and 2100  $\mu\text{g/L}$  concentration, respectively; this is typical of kinetics approaching zeroth order, in which case conversion becomes inversely proportional to the initial concentration. Likewise, the initial (i.e. over the first 5 min) reaction rate is 37.4, 56 and 39.6  $\mu\text{g}/(\text{L min})$  at 260, 525 and 1050  $\mu\text{g/L}$  SMX, respectively, i.e. nearly independent of the initial concentration. At a simple level, the rate of generation of reactive species should solely be a function of photon flux and the catalyst, concentration [24,25] and, therefore, nearly constant for the experiments of Fig. 9. At increased SMX concentrations, the concentration of reactive species becomes the limiting reactant and this explains the observed, near-zeroth order kinetics.

#### 3.5. Effect of the water matrix

Fig. 10 shows SMX degradation efficiency in different matrices including bottled water (BW) and secondary treated wastewater (WW). Degradation in WW at its inherent pH of 8 is completely impeded, which implies the detrimental competition of the organic and inorganic, non-target constituents of WW with SMX for the reactive species in the liquid phase. The experiment was repeated in a 50:50 mixture of UPW:WW showing exactly the same behavior (data not shown for brevity). Degradation in BW at its inherent pH of 7.6 is only partially hindered compared to that in UPW at its inherent pH of 6; the computed rate constant in BW is  $0.1 \text{ min}^{-1}$ , about a third less than in

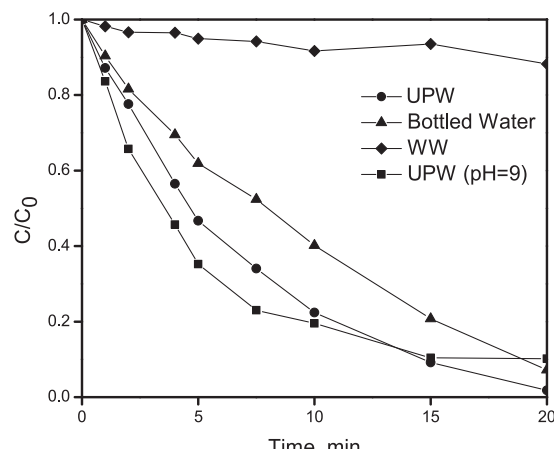


**Fig. 10.** Effect of the water matrix on 525  $\mu\text{g/L}$  SMX degradation with 50 mg/L  $\text{Ag}_3\text{PO}_4/\text{WO}_3(75:25)$ .

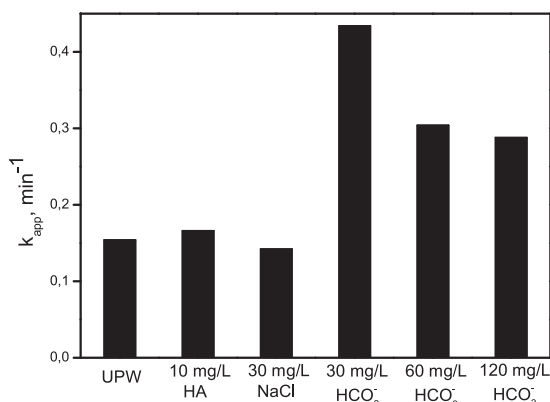


Fig. 11. Effect of bicarbonate, chloride and humic acid on the photocatalytic degradation of 525 µg/L SMX with 50 mg/L  $\text{Ag}_3\text{PO}_4/\text{WO}_3$ (75:25).

UPW. To test whether differences in reactivity are associated with the matrix pH, an additional experiment was performed in UPW with the initial pH adjusted to 9; as seen in Fig. 10, SMX degradation is not practically dependent on initial pH and the computed rate constants are  $0.154$  and  $0.165 \text{ min}^{-1}$  at initial pH of 6 and 9, respectively. This is consistent with the charge of SMX and the catalyst surface at the pH values in question. SMX has two  $pK_a$  values, namely  $pK_{a,1} = 1.85 \pm 0.3$  and  $pK_{a,2} = 5.60 \pm 0.04$  [26], above which SMX is predominantly negatively charged. Moreover, at pH values greater than about 5.4, which is the point of zero charge for  $\text{Ag}_3\text{PO}_4$  [27], its surface becomes negatively charged. In this view, at near-neutral and alkaline conditions both the catalyst surface and SMX are negatively charged and the electrostatic repulsion between them is likely to affect similarly the extent of adsorption and subsequent reaction.

To evaluate the possible role of certain matrix constituents on SMX degradation, experiments were performed spiking UPW with humic acid (HA), chloride or bicarbonate and the results, in the form of apparent rate constants, are given in Fig. 11. The presence of HA, which is typically employed as a model compound of the organic matter occurring in natural waters, has no effect on SMX degradation although its concentration of 10 mg/L (this was chosen to match the organic carbon content of the WW matrix) is two orders of magnitude greater than SMX. This rather unexpected finding implies that other WW components (e.g. extracellular polymers secreted by the microorganisms, non-biodegradable organics) may scavenge the reactive species and/or compete with SMX for the adsorption sites of the catalyst.

Unlike several studies reporting detrimental effects of chloride on the photocatalytic degradation of organics [28], this does not seem to be the case in the present system. The inhibition mechanism associated with chloride ions includes competitive adsorption onto the photocatalyst surface and/or scavenging of the photogenerated holes to form chlorine-containing radicals.

On the contrary, bicarbonate, which is the main ion in natural waters, has a positive impact on SMX degradation; the computed rate constants in the presence of 30–120 mg/L bicarbonate are 2–3 times greater than in UPW. Carbonate and bicarbonate ions react with hydroxyl radicals to form the carbonate radical ( $\text{CO}_3^{\cdot-}$ ). Although the latter ( $E^\circ = 1.78 \text{ V}$  at  $\text{pH} = 7$ ) is a weaker oxidant than the former ( $E^\circ = 2.3 \text{ V}$  at  $\text{pH} = 7$ ) [29], it can selectively react with the aniline moiety of sulfonamides, thus accelerating their decomposition. Furthermore, the carbonate radical is more stable and has longer lifetime than the hydroxyl radical, hence it can diffuse away from the catalyst surface and react in the liquid bulk [30].

These results clearly pinpoint the need and significance to work with actual water matrices rather than UPW. Even synthetic solutions containing certain matrix components may lead to inconclusive results since the interactions amongst the various known and unknown components may not be fully understood.

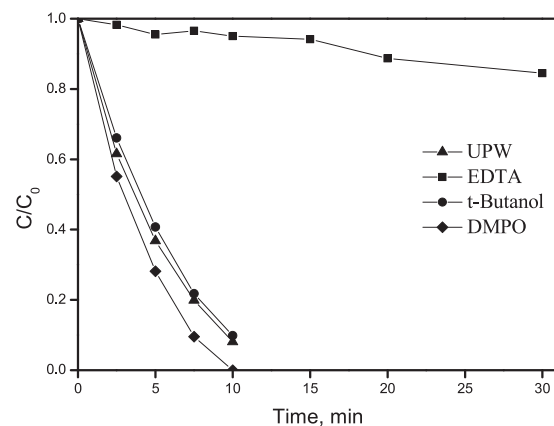


Fig. 12. Effect of various scavengers on the photocatalytic degradation of 525 µg/L SMX with 100 mg/L  $\text{Ag}_3\text{PO}_4/\text{WO}_3$ (75:25). [EDTA] = [t-Butanol] = 10 g/L, [DMPO] = 1 g/L.

### 3.6. Mechanism of SMX degradation

UPLC-ESI-MS analysis was performed to identify possible TPs accompanying SMX degradation. The parent compound shows a molecular ion  $[\text{M} + \text{H}]^+$  ( $\text{C}_{10}\text{H}_{12}\text{O}_3\text{N}_3\text{S}^+$ ) at  $m/z = 254.0596$  ( $\Delta(\text{ppm}) = 0.636$ , ring double bond (RDB) equivalent of 6.5) and a characteristic sodium adduct  $[\text{M} + \text{Na}]^+$  at  $m/z = 276.0414$  ( $\Delta(\text{ppm}) = 0.061$ , RDB = 6.5) in MS spectrum (supplementary information, Fig. S2A). Interestingly, the analysis revealed the complete absence of mono- or poly-hydroxylated TPs, compounds that had been previously identified during the degradation of SMX by various advanced oxidation processes [31–33]; this finding implies the negligible contribution of hydroxyl radicals in the degradation of SMX. In this perspective, additional experiments were performed in the presence of various scavengers, namely t-butanol, DMPO and EDTA, at concentrations which are several orders of magnitude greater than SMX and the results are depicted in Fig. 12. Evidently, the addition of DMPO or t-butanol, typical scavengers of hydroxyl radicals, has practically no effect on SMX degradation; conversely, degradation is nearly completely quenched in the presence of EDTA, which behaves as a hole scavenger [34].

According to previous studies [12,35], the photogenerated holes may directly oxidize organic pollutants (i.e. dyes, bisphenol A) adsorbed on  $\text{Ag}_3\text{PO}_4$  surface. In phosphate oxy-acid salt photocatalysts such as  $\text{BiPO}_4$  and  $\text{Ag}_3\text{PO}_4$ , the holes remain on the surface owing to the large negative charge of the  $\text{PO}_4^{3-}$  ions, while electrons are repelled [35,36]. Hydroxyl radicals generation was scarcely observed during  $\text{Ag}_3\text{PO}_4$  photocatalysis [35], which is consistent with the findings of this work concerning the (i) absence of hydroxylated or oxygenated TPs, and (ii) the zero effect of radical scavengers on SMX degradation. Therefore, it can safely be hypothesized that the photoinduced holes, with a high oxidation potential of + 2.45 V vs. NHE, directly react with SMX.

Two TPs were identified by UPLC-ESI-MS analysis. TP1 shows a molecular ion  $[\text{M} + \text{H}]^+$  ( $\text{C}_6\text{H}_8\text{O}_2\text{NS}^+$ ) at  $m/z = 158.0271$  ( $\Delta(\text{ppm}) = 0.723$ , RDB = 3.5) (supplementary information, Fig. S2B), which is attributed to 4-hydrosulfonylaniline, a compound that has also been detected during SMX degradation by ultrasound/ozone oxidation [37]. Thus, the first degradation pathway can be rationalized via the cleavage of the S–N bond yielding TP1 and 5-amino-3-methyl isoxazole. This mechanism has also been proposed for the photocatalytic degradation of SMX by different photocatalysts [38,39]. TP2 shows a molecular ion  $[\text{M} + \text{H}]^+$  at  $m/z = 227.1754$  and characteristic sodium adduct  $[\text{M} + \text{Na}]^+$  at  $m/z = 249.1574$  (supplementary information, Fig. S2C). Although previous publications on ultrasound/ozone oxidation [37] and permanganate-assisted photooxidation [40] of SMX have reported the formation of a TP with  $m/z = 226.82$ , proposing *N*-ethynyl-

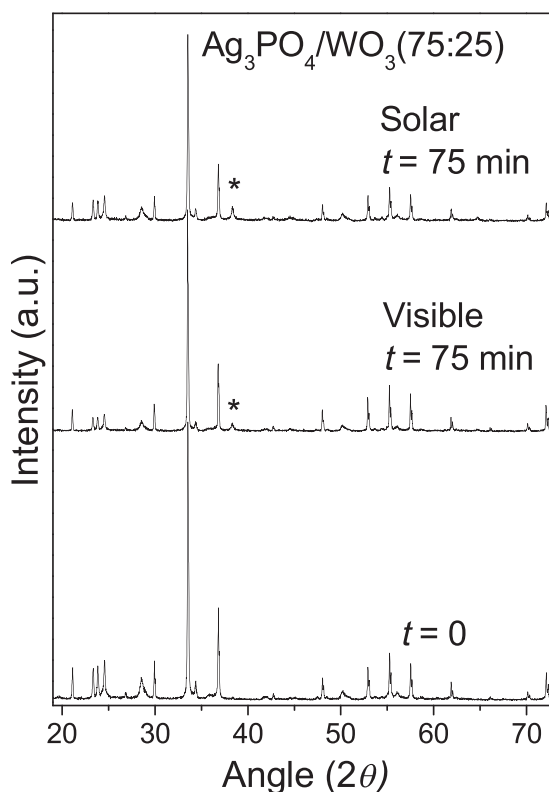


**Fig. 13.** XRD patterns of the  $\text{Ag}_3\text{PO}_4/\text{WO}_3(75:25)$  photocatalyst obtained for the as prepared sample ( $t = 0$ ), and after exposure to solar and visible radiation for 75 min (reusability experiment). The diffraction peaks attributed to metallic Ag are marked with an asterisk (\*). Other peaks are due to  $\text{Ag}_3\text{PO}_4$  and  $\text{WO}_3$  phases, as shown in Fig. 1.

4-nitrobenzenesulfonamide as a probable structure, the use of accurate mass measurements in the present study did not allow the confirmation of the above structure. Based on the observed molecular mass though, the formation of TP2 can be rationalized through the rupture of isoazole ring, a common pathway in photocatalytic processes [33,41].

### 3.7. Catalyst reusability and stability

A final set of experiments were performed to appraise the catalytic activity upon repeated use implementing the procedure as follows: the reaction vessel was fed with 525  $\mu\text{g/L}$  SMX and 100 mg/L fresh  $\text{Ag}_3\text{PO}_4/\text{WO}_3(75:25)$  catalyst and the reaction mixture was subject to solar irradiation for 15 min, at the end of which the residual SMX concentration was measured. The vessel was then re-loaded up to 525  $\mu\text{g/L}$  SMX and the mixture was irradiated for another 15 min and this cycle was repeated five times. The extent of SMX degradation was 100% for the first two cycles but then decreased to 75%, 45% and 30% at the end of cycles 3–5, respectively.

It is well-documented in the literature that  $\text{Ag}_3\text{PO}_4$  suffers photo-corrosion as the photogenerated electrons can reduce  $\text{Ag}_3\text{PO}_4$  to metallic silver [1–3]. This is demonstrated in Fig. 13, where the XRD patterns of the fresh catalyst and after exposure for 75 min to solar and visible radiation are shown; small diffraction peaks attributed to metallic silver clearly appear in the patterns of the used catalyst, confirming that some photo-corrosion has occurred. Similarly, the formation of metallic silver has also been reported by other researchers working with the photocatalytic degradation of dyes over  $\text{Ag}_3\text{PO}_4/\text{WO}_3$  composites [12,13,18]. We have reported [10] similar findings using  $\text{Ag}_3\text{PO}_4/\text{TiO}_2$  composite catalysts for the solar photocatalytic degradation of bisphenol A; the partial loss of catalyst activity was attributed to its partial transformation to metallic silver, the extent of which was dependent on the specific reaction conditions.

An additional experiment was performed with 500 mg/L  $\text{Ag}_3\text{PO}_4/\text{WO}_3(75:25)$  catalyst and 525  $\mu\text{g/L}$  SMX under solar radiation and silver leaching in the liquid phase was measured by ICP-MS; the extent of silver dissolution was 8% and 12.3% after 15 and 75 min of reaction, respectively; the final value corresponds to a silver concentration of 40 mg/L, which exceeds the secondary drinking water regulation threshold of 0.1 mg/L set by USEPA [42].

### 3.8. SMX degradation by $\text{TiO}_2/\text{WO}_3$ photocatalysis and other advanced catalytic processes

In a recent work of our group [31], various  $\text{TiO}_2/\text{WO}_3$  composites were synthesized, characterized and tested for the solar photocatalytic degradation of SMX under comparable experimental conditions. A composite containing 4 wt.%  $\text{WO}_3$  and calcined at 700 °C was the most effective, resulting in apparent rate constants of 0.034 and 0.073  $\text{min}^{-1}$  for the degradation of 350  $\mu\text{g/L}$  SMX at 50 and 100 mg/L catalyst concentration, respectively. The corresponding values for the degradation of 525  $\mu\text{g/L}$  SMX with the  $\text{Ag}_3\text{PO}_4/\text{WO}_3(75:25)$  catalyst (Fig. 8C) are 3.5–4.5 times greater than with the  $\text{TiO}_2/\text{WO}_3$  composite, although the contaminant concentration is 150% greater. Besides differences in reaction rates, SMX degradation occurs through different mechanisms and pathways as evidenced by the identified TPs; titanabased composites favor hydroxyl radical-mediated reactions [31], while silver orthophosphate-based composites favor the participation of holes.

Our group has recently proposed [43] the use of sodium persulfate as a source of sulfate radicals for the degradation of SMX. Notably, persulfate activation can be the result of the combined synergistic action of (i) solar light, and (ii) metal-free biochars derived from valorized waste biomass. This environmentally sustainable process degrades 250  $\mu\text{g/L}$  SMX with 250 mg/L persulfate and 90 mg/L biochar at 0.065  $\text{min}^{-1}$  rate constant.

A major drawback associated with slurry processes is the need to separate the (photo)catalyst from the reactor. Novel magnetic carbon xerogels containing iron and cobalt were prepared and tested for the degradation of SMX by a Fenton-like reaction [44]. Although the rates were substantially lower (i.e. rate constant of ca 0.01  $\text{min}^{-1}$  for the degradation of 500  $\mu\text{g/L}$  SMX with 500 mg/L  $\text{H}_2\text{O}_2$  and 40 mg/L catalyst at 25 °C) than those achieved in photochemical studies (i.e. in Refs. [31] and [43], as well as in this work), the catalyst could be fully recovered magnetically post-treatment.

### 4. Conclusions

A series of  $\text{Ag}_3\text{PO}_4/\text{WO}_3$  composites with different  $\text{Ag}_3\text{PO}_4:\text{WO}_3$  molar ratios were prepared, characterized and tested for the photocatalytic degradation of sulfamethoxazole, a micro-contaminant of emerging environmental concern. The main conclusions are as follows:

- (1) Photocatalytic activity strongly depends on the  $\text{Ag}_3\text{PO}_4:\text{WO}_3$  molar ratio. The photocatalyst with a 75:25 ratio was substantially more active for SMX degradation than the rest, i.e. those with 85:15, 60:40 40:60 and 25:75 ratios; this may be attributed, at least in part, to the greater crystallinity of the  $\text{Ag}_3\text{PO}_4/\text{WO}_3(75:25)$  sample. On the other hand, photocatalyst composition seems not to affect appreciably other properties such as specific surface area, mean primary crystallite size and energy band gap.
- (2) Besides photocatalyst composition, the kinetics of SMX degradation depend on several operating factors, including catalyst and SMX concentration, type of irradiation and the water matrix. Reactions in UPW are faster than in actual matrices (i.e. bottled water and wastewater), signifying possible interactions amongst the matrix constituents, the substrate and the photocatalyst. Although SMX degradation occurs to a substantial degree under visible light only, the contribution of the ultraviolet part of the solar spectrum is still

important, especially at lower catalyst concentrations.

(3) The title reaction seems to proceed through the oxidative action of the photogenerated holes, while the role of hydroxyl radicals is insignificant; this is manifested by the effect of various scavengers on SMX degradation, as well the absence of hydroxylated or oxygenated TP.

(4) Despite the excellent performance of the fresh  $\text{Ag}_3\text{PO}_4/\text{WO}_3$ (75:25) photocatalyst (which is an order of magnitude greater than that of P-25  $\text{TiO}_2$ ), its activity decreases upon repeated use. This can be assigned to (i) photo-corrosion of the catalyst involving the reduction of silver phosphate to metallic silver, and (ii) partial dissolution of silver in the aqueous phase.

## Acknowledgements

The authors wish to thank (i) N.P. Nikolaidis and M.L. Saru (Technical University of Crete, Laboratory of Hydrogeochemical Engineering and Remediation of Soils) for performing ICP-MS analysis; (ii) M. Kollia and A.K. Seferlis, staff of the Laboratory of Electron Microscopy and Microanalysis (L.E.M.M.) at University of Patras; (iii) the unit of environmental, organic and biochemical high resolution-Orbitrap-LC-MS analysis of the University of Ioannina for providing access to the instrumentation facilities.

## Appendix A. Supplementary data

Supplementary material related to this article can be found, in the online version, at doi:<https://doi.org/10.1016/j.apcatb.2018.03.011>.

## References

- [1] G.F. Huang, Z.L. Ma, W.Q. Huang, Y. Tian, C. Jiao, Z.M. Yang, Z. Wan, A. Pan, *J. Nanomater* 2013 (2013) 1–8.
- [2] Z. Yi, J. Ye, N. Kikugawa, T. Kako, S. Ouyang, H. Stuart-Williams, H. Yang, J. Cao, W. Luo, Z. Li, Y. Liu, R.L. Withers, *Nat. Mater.* 9 (2010) 559–564.
- [3] Y.Z. Ma, F. Cheng, W.S. Liu, J. Wang, Y.K. Wang, T. Nonferr, *Metal Soc.* 25 (2015) 112–121.
- [4] J. Cao, B. Luo, H. Lin, B. Xu, S. Chen, J. Hazard. Mater. 217–218 (2012) 107–115.
- [5] Y. Liu, L. Fang, H. Lu, Y. Li, C. Hu, H. Yu, *Appl. Catal. B-Environ.* 115–116 (2012) 245–252.
- [6] W. Yao, B. Zhang, C. Huang, C. Ma, X. Song, Q. Xu, *J. Mater. Chem.* 22 (2012) 4050–4055.
- [7] J.-W. Xu, Z.-D. Gao, K. Han, Y. Liu, Y.-Y. Song, *ACS Appl. Mater. Interfaces* 6 (2014) 15122–15131.
- [8] F.-M. Zhao, L. Pan, S. Wang, Q. Deng, J.-J. Zou, L. Wang, X. Zhang, *Appl. Surf. Sci.* 317 (2014) 833–838.
- [9] Z. Frontistis, M. Antonopoulou, A. Petala, D. Venieri, I. Konstantinou, D.I. Kondarides, D. Mantzavinos, *J. Hazard. Mater.* 323 (2017) 478–488.
- [10] M.E. Taheri, A. Petala, Z. Frontistis, D. Mantzavinos, D.I. Kondarides, *Catal. Today* 280 (2017) 99–107.
- [11] J.J. Liu, X.L. Fu, S.F. Chen, Y.F. Zhu, *Appl. Phys. Lett.* 99 (2011) 191903.
- [12] J. Zhang, K. Yu, Y. Yu, L.L. Lou, Z. Yang, J. Yang, S. Liu, *J. Mol. Catal. A-Chem.* 391 (2014) 12–18.
- [13] Y. Chang, K. Yu, C. Zhang, R. Li, P. Zhao, L.-L. Lou, S. Liu, *Appl. Catal. B-Environ.* 176–177 (2015) 363–373.
- [14] R. Hirsh, T. Ternes, K. Haberer, K.L. Kratz, *Sci. Total Environ.* 225 (1999) 109–118.
- [15] T. Heberer, *Toxicol. Lett.* 131 (2002) 5–17.
- [16] K. Kummerer, *Chemosphere* 75 (2009) 417–434.
- [17] S.E. Jorgensen, B. Halling-Sorensen, *Chemosphere* 40 (2000) 691–699.
- [18] C. Wang, M. Wu, M. Yan, H. Shen, F. Cai, B. Hu, W. Shi, *Ceram. Int.* 41 (2015) 6784–6792.
- [19] H. Xu, H. Zhao, Y. Xu, Z. Chen, L. Huang, Y. Li, Y. Song, Q. Zhang, H. Li, *Ceram. Int.* 42 (2016) 1392–1398.
- [20] J. Lu, Y. Wang, F. Liu, L. Zhang, S. Chai, *Appl. Surf. Sci.* 393 (2017) 180–190.
- [21] L. Cai, X. Xiong, N. Liang, Q. Long, *Appl. Surf. Sci.* 353 (2015) 939–948.
- [22] H. Kisch, S. Sakthivel, M. Janczarek, D. Mitoraj, *J. Phys. Chem. C* 111 (2007) 11445–11449.
- [23] M.N. Abellán, J. Giménez, S. Espigas, *Catal. Today* 144 (2009) 131–136.
- [24] D. Dimitrakopoulou, I. Rethemiotaki, Z. Frontistis, N.P. Xekoukoulotakis, D. Venieri, D. Mantzavinos, *J. Environ. Manage.* 98 (2012) 168–174.
- [25] J. Kulas, I. Rousar, J. Krysa, J. Jirkovski, *J. Appl. Electrochem.* 28 (1998) 843–853.
- [26] N.P. Xekoukoulotakis, C. Drosou, C. Brebou, E. Chatzisymeon, E. Hapeshi, D. Fatta-Kassinos, D. Mantzavinos, *Catal. Today* 161 (2011) 163–168.
- [27] G. Ming, *Chin. J. Catal.* 35 (2014) 1410–1417.
- [28] M. Krivec, R. Dillert, D.W. Bahmann, A. Mehle, J. Strancar, G. Drazic, *Phys. Chem. Chem. Phys.* 16 (2014) 14867–14873.
- [29] D.B. Medinas, G. Cerchiaro, D.F. Trindade, O. Augusto, *IUBMB Life* 59 (2007) 255–262.
- [30] L. Hu, P.M. Flanders, P.L. Miller, T.J. Strathmann, *Water Res.* 41 (2007) 2612–2626.
- [31] E. Ioannidou, Z. Frontistis, M. Antonopoulou, D. Venieri, I. Konstantinou, D.I. Kondarides, D. Mantzavinos, *Chem. Eng. J.* 318 (2017) 143–152.
- [32] S. Gao, Z. Zhao, Y. Xu, J. Tian, H. Qi, W. Lin, F. Cui, J. Hazard. Mater. 274 (2014) 258–269.
- [33] A.G. Trovo, R.F. Nogueira, A. Aguera, C. Sirtori, A.R. Fernandez-Alba, *Chemosphere* 77 (2009) 1292–1298.
- [34] T. Liu, L. Wang, X. Lu, J. Fan, X. Cai, B. Gao, R. Miao, J. Wang, Y. Lv, *RSC Adv.* 7 (2017) 12292–12300.
- [35] H. Katsumata, M. Taniguchi, S. Kaneko, T. Suzuki, *Catal. Commun.* 34 (2013) 30–34.
- [36] C.S. Pan, Y.F. Zhu, *Environ. Sci. Technol.* 44 (2010) 5570–5574.
- [37] W.Q. Guo, R.L. Yin, X.J. Zhou, J.S. Du, H.O. Cao, S.S. Yang, N.Q. Ren, *Ultrason. Sonochem.* 22 (2015) 182–187.
- [38] Y. Song, J. Tian, S. Gao, P. Shao, J. Qi, F. Cui, *Appl. Catal. B-Environ.* 210 (2017) 88–96.
- [39] R. Zanella, E. Avella, R.M. Ramirez-Zamora, F. Castillon-Barraza, J.C. Duran-Alvarez, *Environ. Technol.* (2017), <http://dx.doi.org/10.1080/09593330.2017.1354926> (in press).
- [40] H. Gong, W. Chu, *Chemosphere* 191 (2018) 494–502.
- [41] Q. Hai, J. Hu, J. Hazard. Mater. 323 (2017) 527–536.
- [42] <https://www.water-research.net/index.php/standards/secondary-standards> (Accessed 09 February 2018).
- [43] L. Kemmou, Z. Frontistis, J. Vakros, I.D. Manariotis, D. Mantzavinos, *Catal. Today* (2017), <http://dx.doi.org/10.1016/j.cattod.2017.12.028> (in press).
- [44] R.S. Ribeiro, Z. Frontistis, D. Mantzavinos, D. Venieri, M. Antonopoulou, I. Konstantinou, A.M.T. Silva, J.L. Faria, H.T. Gomes, *Appl. Catal. B-Environ.* 199 (2016) 170–186.